mater.scichina.com link.springer.com

Published online 11 January 2022 | https://doi.org/10.1007/s40843-021-1912-8
Sci China Mater 2022, 65(5): 1262–1268

Dynamic shrinkage of metal-oxygen bonds in atomic Co-doped nanoporous RuO_2 for acidic oxygen evolution

Qiuli Wu[1†], Kang Jiang[1†], Jiuhui Han[2], Dechao Chen[1], Min Luo[3], Jiao Lan[1], Ming Peng[1] and Yongwen Tan[1*]

ABSTRACT **The design of highly active and stable catalysts for the oxygen evolution reaction (OER) in acidic media has become an attractive research area for the development of energy conversion and storage technologies. However, progress in this area has been limited by the poor understanding of the dynamic active structure of catalysts under realistic OER conditions. Here, an atomic Co-doped nanoporous RuO_2 electrocatalyst, which exhibited excellent OER activity and stability in acidic conditions, was synthesized through annealing and etching of a nanoporous Co-Ru alloy. *Operando* X-ray absorption spectroscopy results confirmed that the etching strategy produced abundant oxygen vacancies around the metal centers in the atomic Co-doped nanoporous RuO_2 electrocatalyst. These vacancies created contracted metal-oxygen ligand bonds under realistic OER conditions. The dynamic structural evolution of the synthesized electrocatalyst allowed them to experience lower kinetic barriers during OER catalysis, resulting in enhanced catalytic activity and stability. This study also provided atomic details on the active structure of the electrocatalyst and the influence of their structural evolution on OER activity.**

Keywords: acidic oxygen evolution reaction, nanoporous catalysts, operando X-ray absorption spectroscopy, dynamic structural evolution

INTRODUCTION

The oxygen evolution reaction (OER) plays a critical role in the development of energy conversion and storage technologies, such as electrochemical water splitting, carbon dioxide reduction, and rechargeable metal-air batteries [1–4]. In contrast to alkaline OER, the acidic OER is more attractive due to the higher ionic conductivity and higher-grade purity of the products [5–7]. However, there are many challenges associated with the development of highly active and durable OER electrocatalysts that can operate in acidic media [8–10]. To date, ruthenium oxide (RuO_2)-based materials are one of the most promising acidic OER catalysts. Unfortunately, the poor intrinsic activity and sluggish kinetics of OERs still hinder their practical applications [11–15]. Therefore, rational design of catalysts is required to enhance the OER performance.

A powerful strategy to increase the OER activity of metal oxide catalysts is the introduction of heteroatoms to alter the electronic and geometrical structure of the active sites of the catalyst [16–23]. Particularly, the introduction of heteroatoms into the host lattice generates oxygen vacancies, thus tuning the electronic density of the host element. However, the effects of heteroatoms doped on the catalyst's surface and the nature of the actual catalytic sites remain vague, especially under realistic OER conditions. Therefore, it is highly desirable to develop robust metal-doped catalysts for acidic OER and understand the dynamic behavior of heteroatoms and host atoms in the catalysts.

Here, we rationally designed an atomic Co-doped nanoporous RuO_2 as an acidic OER electrocatalyst, which was prepared by an annealing and electrochemical etching strategy. The atomic Co-doped nanoporous RuO_2 catalyst was endowed with an abundance of oxygen vacancies, as well as three-dimensional (3D) accessibility for reactant molecules. The prepared catalyst exhibited a small overpotential of 169 mV at a current density of 10 mA cm^{-2}, a low Tafel slope of 46 mV dec^{-1}, and excellent durability. These characteristics suggest that the prepared catalyst showed one of the best performances when compared with all reported acidic OER electrocatalysts [16–20]. *Operando* X-ray absorption spectroscopy analyses and density functional theory (DFT) calculations revealed that the dynamic shrinkage of metal-oxygen ligand bonds in the atomic Co-doped RuO_2 not only accelerated the OER kinetics but also led to the formation of the stable surface structure of the catalyst during the OER.

RESULTS AND DISCUSSION

The nanoporous $Co_{20}Ru_{80}$ alloy (denoted as np-$Co_{20}Ru_{80}$) was prepared through electrochemical dealloying of a single-phase $Co_{95}Ru_5$ precursor in an HCl solution (see Method and Figs S1–3 in Supplementary information) [10]. The np-$Co_{20}Ru_{80}$ was then annealed at various temperatures for 4 h in air. The products obtained with treatment under 150, 250, and 350°C were denoted as Co/np-RuO_2-150, Co/np-RuO_2-250, and Co/np-RuO_2-350, respectively. Finally, the cyclic voltammetry (CV) was conducted in the 0.5 mol L^{-1} H_2SO_4 electrolyte to further etch the Co element (Figs S4–6). The corresponding final pro-

[1] College of Materials Science and Engineering, State Key Laboratory of Advanced Design and Manufacturing for Vehicle Body, Hunan University, Changsha 410082, China
[2] Advanced Institute for Materials Research, Tohoku University, Sendai 980-8577, Japan
[3] School of Electronic Information Engineering, Wuxi University, Wuxi 214105, China
[†] These authors contributed equally to the work.
[*] Corresponding author (email: tanyw@hnu.edu.cn)

ducts (catalysts) were denoted as Co_{CV}/np-RuO_2-150, Co_{CV}/np-RuO_2-250, and Co_{CV}/np-RuO_2-350. X-ray diffraction (XRD) patterns of the samples annealed at different temperatures only showed the peaks for RuO_2 and metal Ru (at 150°C) with low crystallinity (Fig. 1a). Meanwhile, annealing at 150°C was not sufficient to completely oxidize Ru, resulting in the presence of metal Ru in the Co_{CV}/np-RuO_2-150. Scanning electron microscopy (SEM) image revealed a nanorod morphology for Co_{CV}/np-RuO_2-250 (Fig. S7). Transmission electron microscopy (TEM) image of Co_{CV}/np-RuO_2-250 revealed the formation of ultrafine ligament and nanoporous structures with a pore size of less than 10 nm (Fig. 1b and Fig. S8). Furthermore, the lattice fringe spaces of rutile RuO_2 (110) were observed (Fig. 1c, d). The selected area electron diffraction (SAED) characterization of Co_{CV}/np-RuO_2-250 showed continuous Debye rings, which can be indexed to the (110), (101), and (200) planes of RuO_2 (Fig. S8). The energy-dispersive X-ray spectroscopy (EDS) elemental mapping demonstrated that Co and Ru elements were uniformly distributed in the catalyst (Fig. 1e). In addition, N_2 adsorption-desorption measurements verified that Co_{CV}/np-RuO_2-250 possessed a large Brunauer-Emmett-Teller (BET) surface area (116.27 $m^2\ g^{-1}$ with an average nanopore size of ca. 5 nm) (Fig. 1f, g).

X-ray photoelectron spectroscopy (XPS) analysis was carried out to assess the chemical state at the surface of the different catalysts. The Ru $3p_{3/2}$ spectra of np-$Co_{20}Ru_{80}$ showed two peaks that were assigned to Ru^0 (461.1 eV) and Ru^{4+} (462.7 eV) (Fig. 2a). The peaks corresponding to the Ru $3p_{3/2}$ peaks of Co/np-RuO_2-250 and Co_{CV}/np-RuO_2-250 were assigned to Ru^{4+} and Ru^{3+} (464.2 eV) [23]. These results suggested the oxidation of Ru after annealing treatment and CV etching. The Co 2p spectra of np-$Co_{20}Ru_{80}$, Co/np-RuO_2-250, and Co_{CV}/np-RuO_2-250 showed the oxidation of Co after the annealing treatment and CV etching, as evidenced by the positive shift of Co 2p peaks for Co/np-RuO_2-250 and Co_{CV}/np-RuO_2-250 (Fig. S9). The O 1s spectra of Co/np-RuO_2-250 and Co_{CV}/np-RuO_2-250 can be divided into four peaks, which corresponded to the lattice O (529.2 eV), OH^- (530.5 eV), oxygen vacancy (O_V) species (531.9 eV), and adsorbed H_2O molecules (533.0 eV) (Fig. 2b) [16]. It was found that the O_V species peak for Co_{CV}/np-RuO_2-250 was much stronger compared with the O_V species peak for Co/np-RuO_2-250. This indicated the increase in the O_V due to CV etching, which may be explained by the electroneutrality principle (i.e., the decrease in the number of cations (Co cation leaching) required a decrease in the number of anions (the loss of O^{2-}) to appropriately balance the charge of catalysts) [16].

X-ray absorption spectroscopy (XAS) was performed to further probe the electronic and atomic structures of the catalysts. Fig. 2c shows the X-ray absorption near-edge structure (XANES) spectra at Ru *k*-edge of Co_{CV}/np-RuO_2-250, together with Co/np-RuO_2-250, Ru foil, and RuO_2. The absorption edge of Co/np-RuO_2-250 was located between those of Ru foil and RuO_2, indicating that the average valence state of Ru in Co/np-RuO_2-250 was between 0 and 4 (see Fig. S10). After CV etching, the Ru species in Co_{CV}/np-RuO_2-250 were further oxidized, as evidenced by the positive shift of absorption edge. Fig. 2d exhibits

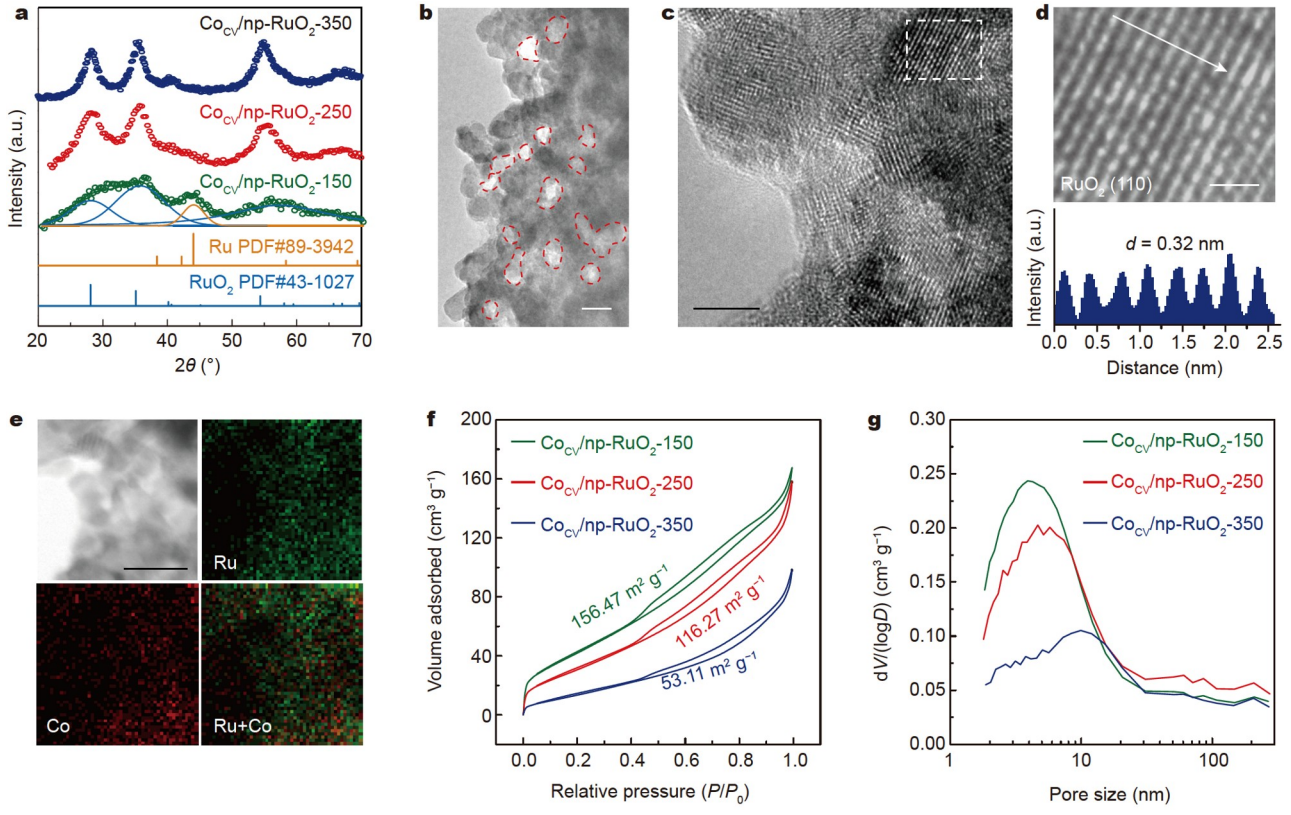

Figure 1 Morphological and structural characterizations of the prepared catalysts: Co_{CV}/np-RuO_2-150, Co_{CV}/np-RuO_2-250, and Co_{CV}/np-RuO_2-350. (a) XRD patterns of the different catalysts. (b) TEM image of Co_{CV}/np-RuO_2-250. (c) High-resolution TEM image of Co_{CV}/np-RuO_2-250. (d) Magnified HRTEM image and the corresponding intensity line profile of Co_{CV}/np-RuO_2-250 from (c). (e) EDS mapping profiles of Co_{CV}/np-RuO_2-250. (f) BET analyses of the different catalysts. (g) Pore size distributions of the different catalysts. Scale bars: 10 nm (b), 5 nm (c), 1 nm (d), and 10 nm (e).

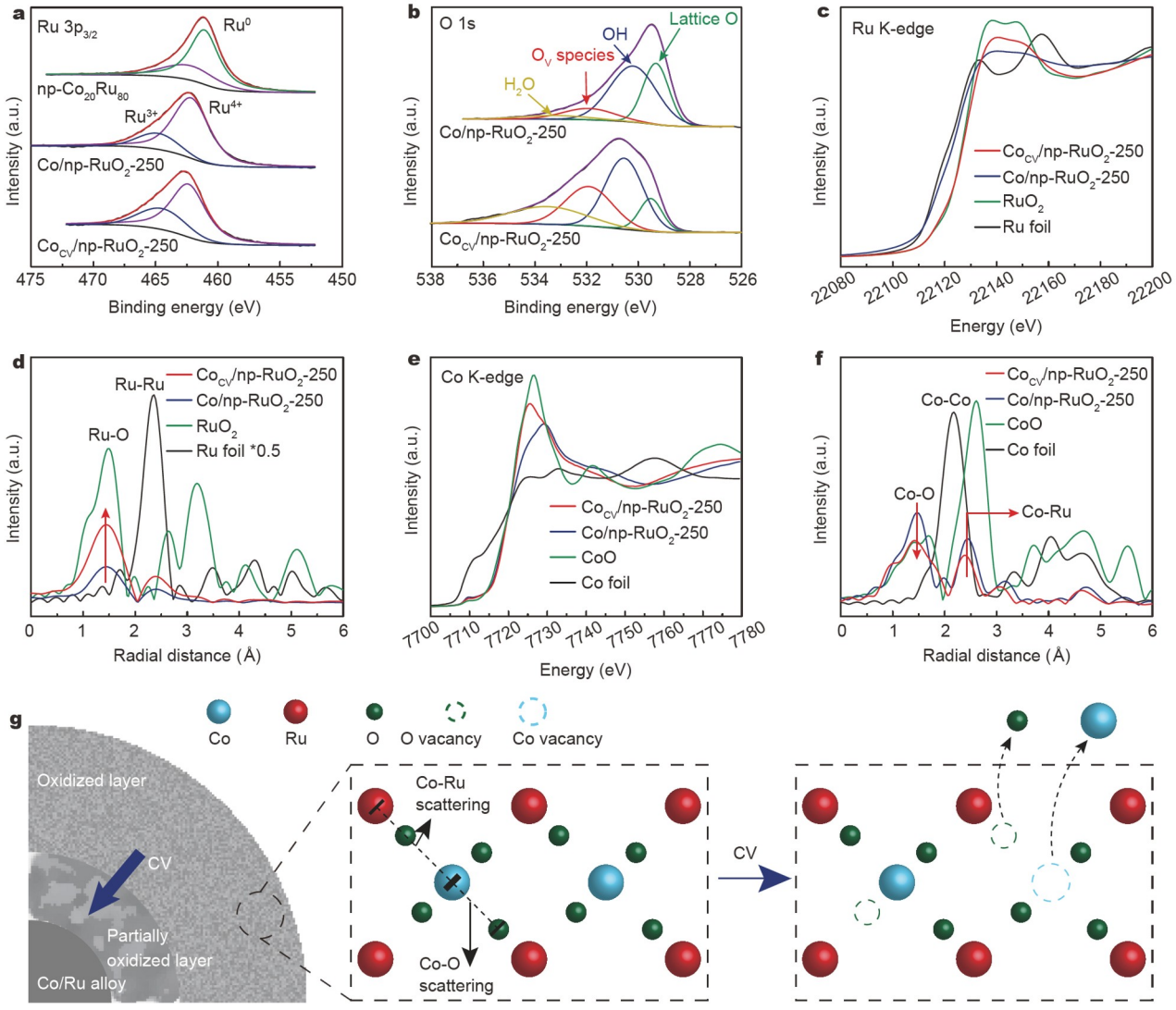

Figure 2 XPS and XAS characterizations of the prepared catalysts. XPS spectra of (a) Ru $3p_{3/2}$ and (b) O 1s regions for np-$Co_{20}Ru_{80}$, Co/np-RuO_2-250, and Co_{CV}/np-RuO_2-250. Ru *k*-edge (c) XANES spectra and (d) the corresponding FT-EXAFS spectra for different catalysts. Co *k*-edge (e) XANES spectra and (f) the corresponding FT-EXAFS spectra for different catalysts. (g) Schematic illustration of the Co leaching and the formation of vacancies during the CV etching process.

the Fourier transforms of extended X-ray absorption fine structure (FT-EXAFS) spectra at Ru *k*-edge of Co_{CV}/np-RuO_2-250 and Co/np-RuO_2-250. The peaks of Co_{CV}/np-RuO_2-250 and Co/np-RuO_2-250 located at ~1.5 Å were assigned to the Ru–O scattering feature. The intensity of Ru–O peak for both Co_{CV}/np-RuO_2-250 and Co/np-RuO_2-250 was much lower than that of RuO_2, which was attributed to the coordination deficiency of Ru [16]. It is worth noting that the Ru–O peak of Co_{CV}/np-RuO_2-250 showed higher peak intensity than that of Co/np-RuO_2-250. This suggested further bulk oxidation during the CV process, which led to the increase in the average Ru–O coordination number. The peak located at ~2.3 Å in the Ru *k*-edge FT-EXAFS spectra was assigned to the Ru–Ru scattering feature. The increase in the Ru–Ru peak intensity after CV etching also indicated a change of the coordination structure for residual alloy clusters due to oxidation. In addition, the Co *k*-edge XANES spectrum of Co/np-RuO_2-250 showed a higher energy absorption edge than that of Co foil, indicating the oxidation of Co species in Co/np-RuO_2-250 (Fig. 2e). The absorption edge of Co_{CV}/np-RuO_2-250 also shifted to higher energy, and this was accompanied by the increase of the white line peak, suggesting the oxidation of residual Co species. The corresponding Co *k*-edge FT-EXAFS spectrum of Co_{CV}/np-RuO_2-250 showed similar scattering features with that of Ru *k*-edge FT-EXAFS spectrum, suggesting the atomic doping of Co into RuO_2 (Fig. 2f and Fig. S11). Meanwhile, the Co *k*-edge FT-EXAFS spectrum of Co_{CV}/np-RuO_2-250 showed a decrease of Co–O peak compared with that of Co/np-RuO_2-250 (Fig. 2f). This confirmed that the oxygen vacancies were created around the residual Co centers after the leaching of Co (Fig. 2g). This not only led to the creation of more active sites but also optimized the electronic structure of RuO_2 [16].

The OER activity of the catalysts was investigated in O_2-saturated 0.5 mol L^{-1} H_2SO_4 by using a typical three-electrode system. Fig. 3a shows the linear sweep voltammetry (LSV) curves of Co_{CV}/np-RuO_2-150, Co_{CV}/np-RuO_2-250, and Co_{CV}/np-RuO_2-350, together with commercial RuO_2 as the benchmark. A notable "decrease-increase" trend in the overpotentials of the

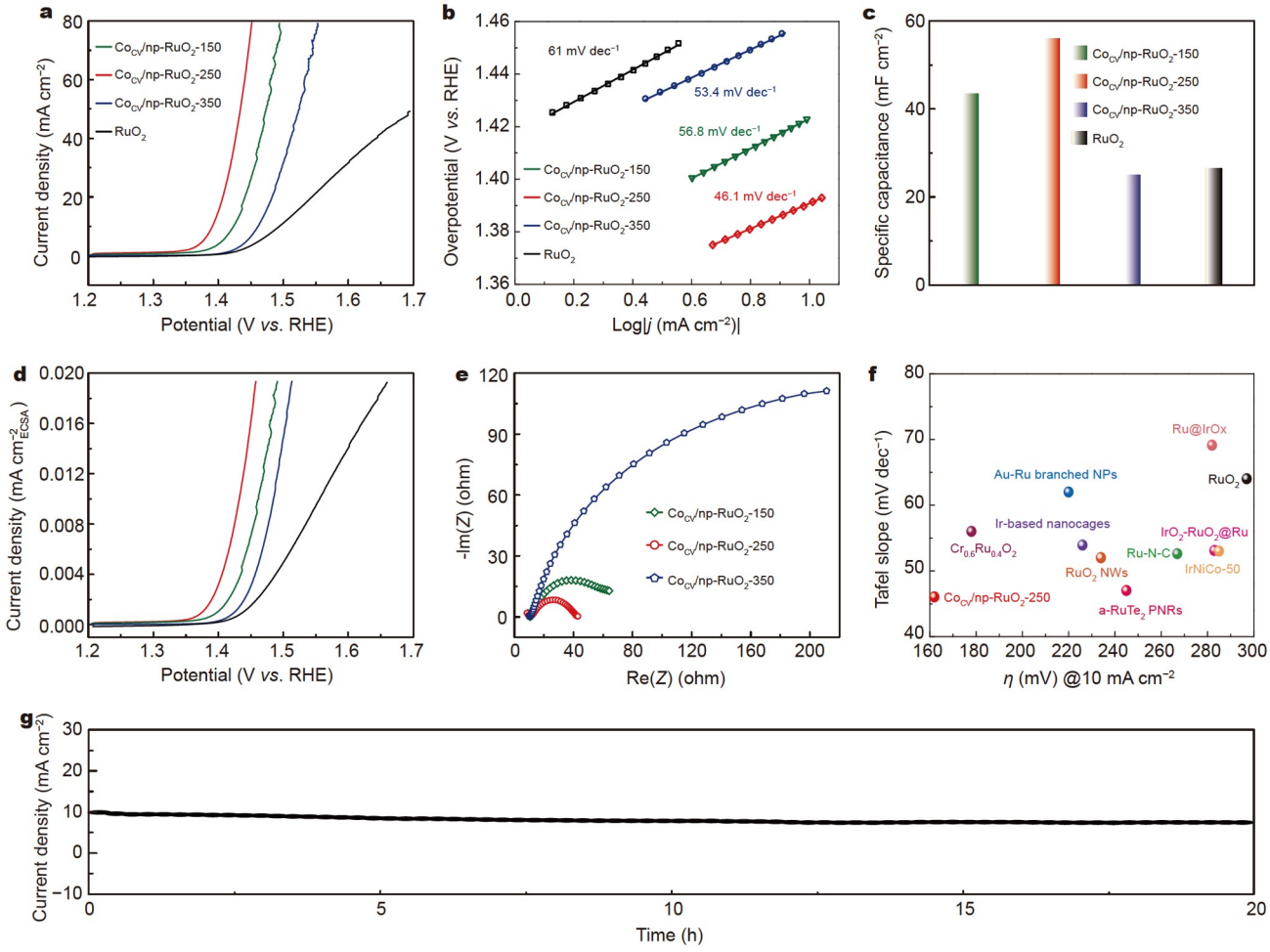

Figure 3 OER performance of the studied catalysts. (a) OER polarization curves of Co_{CV}/np-RuO_2-150, Co_{CV}/np-RuO_2-250, Co_{CV}/np-RuO_2-350, and RuO_2 in 0.5 mol L^{-1} H_2SO_4. (b) The corresponding Tafel plots from (a). (c) Double-layer capacitances (C_{dl}) of different catalysts. (d) The corresponding ECSA-normalized polarization curves from (a). (e) Nyquist plots of different catalysts. (f) The comparisons of kinetics (Tafel slope) and activity (the overpotential required to achieve 10 mA cm^{-2}). (g) Time-dependent current density curve under static overpotential of Co_{CV}/np-RuO_2-250 in acidic electrolyte.

catalysts was observed with the increase of annealing temperature from 150 to 350°C. The Co_{CV}/np-RuO_2-250 showed the best OER performance in terms of the extremely low overpotential of 169 mV at the applied current density of 10 mA cm^{-2}. This value was 31, 61, and 101 mV lower than those obtained from Co_{CV}/np-RuO_2-150, Co_{CV}/np-RuO_2-350, and RuO_2, respectively. A small Tafel slope of 46.1 mV dec^{-1} was derived for Co_{CV}/np-RuO_2-250. This value was significantly lower than those obtained for Co_{CV}/np-RuO_2-150, Co_{CV}/np-RuO_2-350, and RuO_2 (Fig. 3b). The electrochemical double-layer capacitance (C_{dl}) measurements showed the largest C_{dl} value for Co_{CV}/np-RuO_2-250 when compared with the other prepared catalyst (Fig. 3c and Fig. S12), suggesting that more accessible active sites were constructed on Co_{CV}/np-RuO_2-250. After normalizing the current density to the electrochemical active surface area (ECSA), the Co_{CV}/np-RuO_2-250 still produced the highest current density among the prepared catalysts, emphasizing the high intrinsic activity of Co_{CV}/np-RuO_2-250 (Fig. 3d). Furthermore, the electrochemical impedance spectroscopy (EIS) measurements revealed the smallest charge transfer resistance obtained with Co_{CV}/np-RuO_2-250 compared with the other prepared catalysts (Fig. 3e). According to the above results, the Co_{CV}/np-RuO_2-250 also exhibited superior OER performance when compared with the available Ru-based and Ir-based OER catalysts in acidic solution (Fig. 3f and Table S1) [4,7,19,24–27]. Moreover, the chronoamperometry durability test of Co_{CV}/np-RuO_2-250 revealed that it was stable for 20 h in 0.5 mol L^{-1} H_2SO_4 (Fig. 3g).

To understand the high OER activity and stability of the Co_{CV}/np-RuO_2-250 catalyst, *operando* XAS analyses were performed on this catalyst under realistic OER and open-circuit voltage (OCV) conditions, which is an attractive technique for exploring the dynamic structure of catalysts [21,28,29]. As shown in Fig. 4a, the shift to the higher energy of the absorption edge of Ru *k*-edge XANES spectra of the catalyst was higher in the OER than in the OCV conditions. This suggested the increase of the oxidation state for Ru species in the OER conditions. Meanwhile, the Ru–O peaks in the corresponding FT-EXAFS spectra displayed a low-*R* shift in the OER conditions, which indicated a shrinkage of Ru–O bonds (Fig. 4b). The *operando* Co *k*-edge XANES spectra of Co_{CV}/np-RuO_2-250 obtained under realistic OER conditions showed similar changes to that of the *operando* Ru *k*-edge XANES spectra (Fig. 4c). This suggested the oxidation of Co during OER. In addition, the spectra in the inset of Fig. 4c show no change in peak A but a decrease in the peak intensity of peak B under higher applied voltage (1.5 V *vs.* reversible

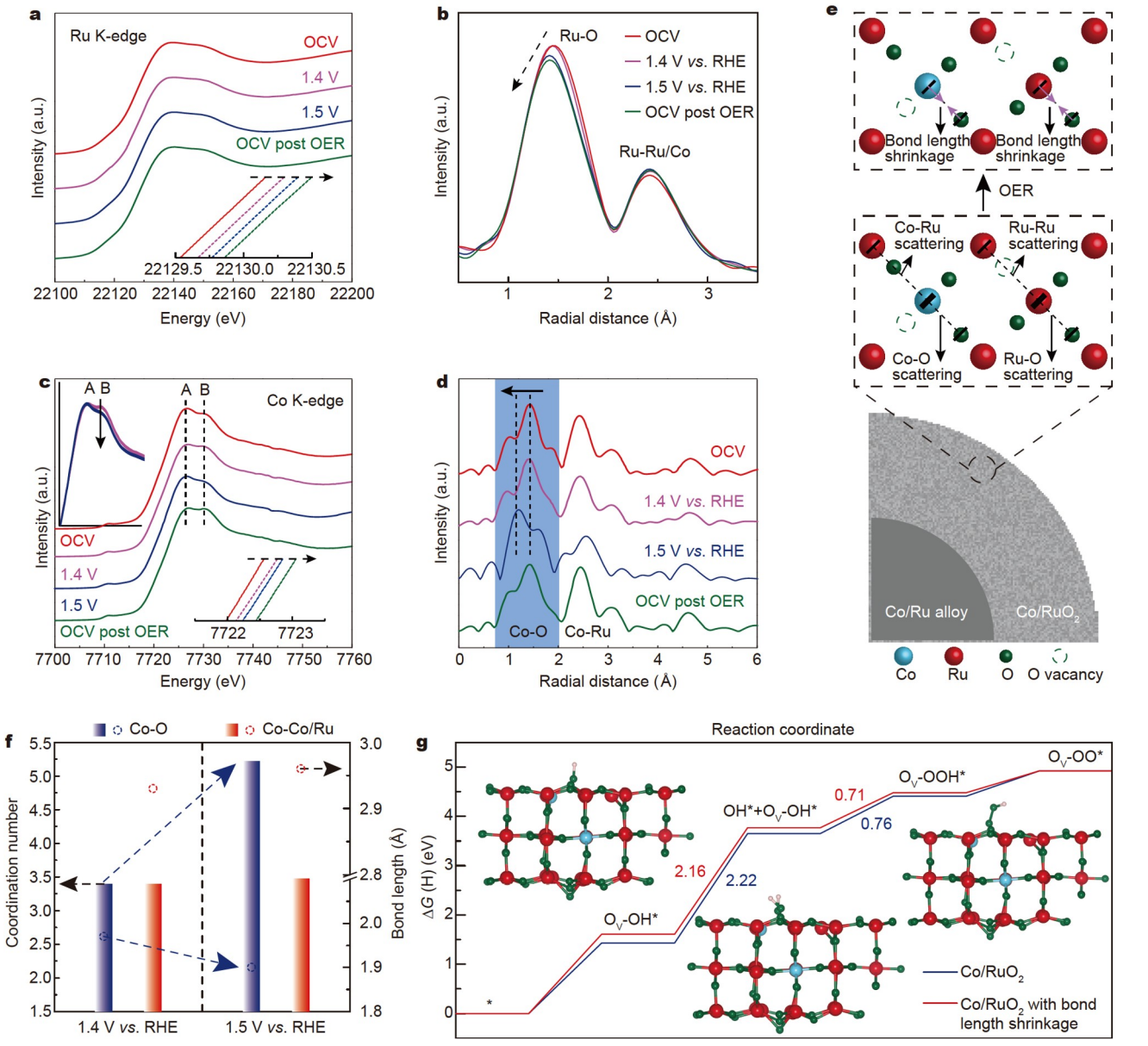

Figure 4 Figure 4 Operando XAS measurements and DFT calculations for the Co_{CV}/np-RuO_2-250 catalyst. *Operando* Ru *k*-edge XANES spectra (a) and the corresponding FT-EXAFS spectra (b) collected under OCV, 1.4 V *vs.* RHE, and 1.5 V *vs.* RHE. *Operando* Co *k*-edge XANES spectra (c) and the corresponding FT-EXAFS spectra (d) collected under OCV, 1.4 V *vs.* RHE, and 1.5 V *vs.* RHE. (e) Schematic illustration of the OER mechanism determined by the *operando* XAS analyses. (f) FT-EXAFS fitting results from (d). (g) The calculated free energy diagrams of the LOM mechanism.

hydrogen electrode (RHE)). This suggested a change in the coordination structure of the catalyst. This can be further confirmed by the corresponding FT-EXAFS spectra (Fig. 4d), which show a sharp shrinkage of the Co–O bonds under the applied voltage of 1.5 V *vs.* RHE. It should also be noted that the Co–O bonds showed greater shrinkage than the Ru–O bonds under realistic OER conditions. This was attributed to the different properties of different metal-oxygen ligand bonds and the more stable Ru–O ligand bonds in the host lattice compared with the Co–O ligand bonds of Co dopant atoms. Based on the *ex-situ* results (see Fig. 2g), the Co leaching during the CV etching produced abundant holes on the oxygen ligands of Co and Ru. The resulting metal-oxygen ligand bonds are most likely shortened under realistic OER conditions, which may play a crucial role in the excellent activity of catalysts (Fig. 4e) [30]. In addition, the stable surface structure resulted from the shortening of metal-oxygen ligand bonds is beneficial to enhancing the stability of the catalyst during the OER conditions [31]. To further study the structure-activity relationships, the FT-EXAFS fitting was performed (Fig. 4f). The results suggested the shrinkage of Co–O bonds from 1.97 to 1.90 Å with the increase of applied voltage (Fig. S13 and Table S2). Based on these changes, DFT calculations were employed to assess the role of bond shrinkage in the OER process (see Methods in Supplementray information). The Co/RuO_2 models with and without bond shrinkage were established according to the FT-EXAFS fitting results. The O vacancies (O_V) were identified as the active sites, and the lattice oxygen oxidation mechanism (LOM) was calculated [16,32,33] (Fig. 4g). The formation of (OH)-O_V-(OH) after the second H_2O attack was identified as the rate-determining step

(RDS). The shortening of metal-oxygen ligand bonds not only reduced the free energy barrier of RDS but also lowered the energy barrier of O-O coupling (the formation of OOH*). These suggested a more favorable OER kinetics under high applied voltage conditions.

CONCLUSION

In conclusion, we developed an atomic Co-doped nanoporous RuO_2 catalyst with abundant oxygen vacancies around the Co centers for OER in acidic media. The prepared Co_{CV}/np-RuO_2-250 catalyst exhibited remarkable catalytic activity and stability toward OER in acidic solutions, outperforming most of the reported electrocatalysts, including IrO_2-based and RuO_2-based materials. *Operando* XAS studies showed the dynamic shortening of the metal-oxygen ligand bonds in Co_{CV}/np-RuO_2-250 under realistic OER conditions. DFT calculations confirmed that the shorter metal-oxygen ligand bonds were probably responsible for the higher intrinsic activity and stability of the prepared catalyst. The shorter ligand bonds reduced the free energy barrier of RDS, thus creating a favorable OER environment. The proposed mechanisms in this work could significantly help in the rational design and synthesis of high-performance acidic OER electrocatalysts.

Received 26 August 2021; accepted 29 November 2021; published online 11 January 2022

1 Seh ZW, Kibsgaard J, Dickens CF, *et al.* Combining theory and experiment in electrocatalysis: Insights into materials design. Science, 2017, 355: eaad4998
2 Seitz LC, Dickens CF, Nishio K, *et al.* A highly active and stable IrO_x/$SrIrO_3$ catalyst for the oxygen evolution reaction. Science, 2016, 353: 1011–1014
3 Chatti M, Gardiner JL, Fournier M, *et al.* Intrinsically stable *in situ* generated electrocatalyst for long-term oxidation of acidic water at up to 80°C. Nat Catal, 2019, 2: 457–465
4 Wang J, Han L, Huang B, *et al.* Amorphization activated ruthenium-tellurium nanorods for efficient water splitting. Nat Commun, 2019, 10: 5692
5 Yang J, Ji Y, Shao Q, *et al.* A universal strategy to metal wavy nanowires for efficient electrochemical water splitting at pH-universal conditions. Adv Funct Mater, 2018, 28: 1803722
6 Lin Y, Tian Z, Zhang L, *et al.* Chromium-ruthenium oxide solid solution electrocatalyst for highly efficient oxygen evolution reaction in acidic media. Nat Commun, 2019, 10: 162
7 Shan J, Guo C, Zhu Y, *et al.* Charge-redistribution-enhanced nanocrystalline Ru@IrO_x electrocatalysts for oxygen evolution in acidic media. Chem, 2019, 5: 445–459
8 Kim JS, Kim B, Kim H, *et al.* Recent progress on multimetal oxide catalysts for the oxygen evolution reaction. Adv Energy Mater, 2018, 8: 1702774
9 Zhao ZL, Wang Q, Huang X, *et al.* Boosting the oxygen evolution reaction using defect-rich ultra-thin ruthenium oxide nanosheets in acidic media. Energy Environ Sci, 2020, 13: 5143–5151
10 Zhao Y, Luo M, Chu S, *et al.* 3D nanoporous iridium-based alloy microwires for efficient oxygen evolution in acidic media. Nano Energy, 2019, 59: 146–153
11 Bhowmik T, Kundu MK, Barman S. Growth of one-dimensional RuO_2 nanowires on g-carbon nitride: An active and stable bifunctional electrocatalyst for hydrogen and oxygen evolution reactions at all pH values. ACS Appl Mater Interfaces, 2016, 8: 28678–28688
12 DeSario PA, Chervin CN, Nelson ES, *et al.* Competitive oxygen evolution in acid electrolyte catalyzed at technologically relevant electrodes painted with nanoscale RuO_2. ACS Appl Mater Interfaces, 2017, 9: 2387–2395
13 Cui X, Ren P, Ma C, *et al.* Robust interface Ru centers for high-performance acidic oxygen evolution. Adv Mater, 2020, 32: 1908126
14 Audichon T, Guenot B, Baranton S, *et al.* Effect of the annealing atmosphere on the electrochemical properties of RuO_2 nano-oxides synthesized by the instant method. Appl Catal B-Environ, 2017, 218: 385–397
15 Su J, Ge R, Jiang K, *et al.* Assembling ultrasmall copper-doped ruthenium oxide nanocrystals into hollow porous polyhedra: Highly robust electrocatalysts for oxygen evolution in acidic media. Adv Mater, 2018, 30: 1801351
16 Tian Y, Wang S, Velasco E, *et al.* A Co-doped nanorod-like RuO_2 electrocatalyst with abundant oxygen vacancies for acidic water oxidation. iScience, 2020, 23: 100756
17 Chen S, Huang H, Jiang P, *et al.* Mn-doped RuO_2 nanocrystals as highly active electrocatalysts for enhanced oxygen evolution in acidic media. ACS Catal, 2019, 10: 1152–1160
18 Retuerto M, Pascual L, Calle-Vallejo F, *et al.* Na-doped ruthenium perovskite electrocatalysts with improved oxygen evolution activity and durability in acidic media. Nat Commun, 2019, 10: 2041
19 Wang J, Ji Y, Yin R, *et al.* Transition metal-doped ultrathin RuO_2 networked nanowires for efficient overall water splitting across a broad pH range. J Mater Chem A, 2019, 7: 6411–6416
20 González-Huerta RG, Ramos-Sánchez G, Balbuena PB. Oxygen evolution in Co-doped RuO_2 and IrO_2: Experimental and theoretical insights to diminish electrolysis overpotential. J Power Sources, 2014, 268: 69–76
21 Jiang K, Luo M, Peng M, *et al.* Dynamic active-site generation of atomic iridium stabilized on nanoporous metal phosphides for water oxidation. Nat Commun, 2020, 11: 2701
22 Wu G, Chen W, Zheng X, *et al.* Hierarchical Fe-doped NiO_x nanotubes assembled from ultrathin nanosheets containing trivalent nickel for oxygen evolution reaction. Nano Energy, 2017, 38: 167–174
23 Ge R, Li L, Su J, *et al.* Ultrafine defective RuO_2 electrocatayst integrated on carbon cloth for robust water oxidation in acidic media. Adv Energy Mater, 2019, 9: 1901313
24 Cao L, Luo Q, Chen J, *et al.* Dynamic oxygen adsorption on single-atomic ruthenium catalyst with high performance for acidic oxygen evolution reaction. Nat Commun, 2019, 10: 4849
25 Li G, Li S, Ge J, *et al.* Discontinuously covered IrO_2–RuO_2@Ru electrocatalysts for the oxygen evolution reaction: How high activity and long-term durability can be simultaneously realized in the synergistic and hybrid nano-structure. J Mater Chem A, 2017, 5: 17221–17229
26 Zaman WQ, Wang Z, Sun W, *et al.* Ni–Co codoping breaks the limitation of single-metal-doped IrO_2 with higher oxygen evolution reaction performance and less iridium. ACS Energy Lett, 2017, 2: 2786–2793
27 Zhu J, Chen Z, Xie M, *et al.* Iridium-based cubic nanocages with 1.1-nm-thick walls: A highly efficient and durable electrocatalyst for water oxidation in an acidic medium. Angew Chem Int Ed, 2019, 58: 7244–7248
28 Jiang K, Luo M, Liu Z, *et al.* Rational strain engineering of single-atom ruthenium on nanoporous MoS_2 for highly efficient hydrogen evolution. Nat Commun, 2021, 12: 1687
29 Yu Y, Jiang K, Luo M, *et al.* Self-activated catalytic sites on nanoporous dilute alloy for high-efficiency electrochemical hydrogen evolution. ACS Nano, 2021, 15: 5333–5340
30 Nong HN, Reier T, Oh HS, *et al.* A unique oxygen ligand environment facilitates water oxidation in hole-doped $IrNiO_x$ core–shell electrocatalysts. Nat Catal, 2018, 1: 841–851
31 Li P, Wang M, Duan X, *et al.* Boosting oxygen evolution of single-atomic ruthenium through electronic coupling with cobalt-iron layered double hydroxides. Nat Commun, 2019, 10: 1711
32 Huang ZF, Song J, Du Y, *et al.* Chemical and structural origin of lattice oxygen oxidation in Co–Zn oxyhydroxide oxygen evolution electrocatalysts. Nat Energy, 2019, 4: 329–338
33 Huang ZF, Song J, Dou S, *et al.* Strategies to break the scaling relation toward enhanced oxygen electrocatalysis. Matter, 2019, 1: 1494–1518

Acknowledgements The authors acknowledge the support from the National Natural Science Foundation of China (51771072), the Outstanding

Youth Scientist Foundation of Hunan Province (2020JJ2006), the Fundamental Research Funds for the Central Universities, and the State Key Laboratory of Advanced Design and Manufacturing for Vehicle Body Independent Research Project (71860007). The authors also thank Dr. Ying-Rui Lu and Prof. Ting-Shan Chan for the XAS measurement at Taiwan Light Source.

Author contributions Tan Y conceived and supervised this study; Wu Q, Jiang K, Chen D and Lan J carried out the fabrication and characterizations of materials, and electrochemical measurements; Han J conducted the TEM characterizations; Jiang K and Peng M contributed to the XAS measurements and analyses; Tan Y, Jiang K, and Wu Q wrote the paper. All authors contributed to discussions and manuscript review.

Conflict of interest The authors declare no conflict of interest.

Supplementary information Experimental details and supporting data are available in the online version of the paper.

Qiuli Wu received her MSc degree from Hunan University under the supervisor of Prof. Tan in 2020. Her research interests mainly focus on the preparation and application of nanoporous materials.

Kang Jiang is currently a PhD student under the supervisor of Prof. Tan at the College of Materials Science and Engineering, Hunan University. He received his BE degree from Hunan University in 2018. His current research focuses on the design of 3D nanoporous materials and their applications in electrocatalytic water splitting.

Yongwen Tan is a full professor at the College of Materials Science and Engineering, Hunan University. He received his PhD degree from the College of Materials Science and Engineering, Shanghai Jiao Tong University, China, in 2013. Then, he joined the Advanced Institute for Materials Research (AIMR), Tohoku University as a research associate. His research focuses on the synthesis and applications of 3D nanoporous materials.

原子级Co掺杂纳米多孔RuO_2催化剂中金属-氧配体键的动态收缩加速酸性氧析出反应

吴秋丽[1†], 蒋康[1†], 韩久慧[2], 陈德超[1], 罗敏[3], 蓝蛟[1], 彭鸣[1], 谭勇文[1*]

摘要 设计在酸性介质中具有高活性和高稳定性的氧析出反应(OER)催化剂对能量转换和储存技术的发展具有重要意义. 然而, 在实际OER条件下催化剂的原子结构会发生变化, 且目前对其动态活性结构的认识仍然不足. 本文中, 我们通过退火和蚀刻纳米多孔Co-Ru合金合成了具有优异酸性OER活性和稳定性的原子级Co掺杂纳米多孔RuO_2催化剂. 原位X射线吸收光谱证实: 蚀刻策略可以在原子级Co掺杂纳米多孔RuO_2的金属中心周围产生丰富的氧空位, 从而在实际OER条件下产生收缩的金属-氧配体键. 这种动态结构演变降低了催化活性位点在OER过程中的动力学势垒, 因而催化剂的催化活性和稳定性大幅提高. 本研究结果揭示了催化剂活性结构的原子细节以及它们的结构演化对催化活性的影响.

